

Submitted to Journal of Nanoscience and Nanotechnology (Revised version)

Influence of Citric Acid on SnO₂ Nanoparticles Synthesized by Wet Chemical Processes

Lucky M Sikhwivhilu¹, Sreejarani K Pillai¹, Thembela K Hillie^{1,2*}

¹ *DST/CSIR Nanotechnology Innovation Centre, National Centre for Nano-Structured
Materials, CSIR, PO Box 395, Pretoria 0001, South Africa*

² *Department of Physics, University of the Free State, P.O. Box 339 (IB51),
Bloemfontein, ZA9300, South Africa.*

* Corresponding author
Tel.: +27 12 841 3874; Fax: +27 12 841 2229
E-mail: thillie@csir.co.za

Abstract

Tin oxide (SnO_2) nanoparticles with size range of 19 to 100 nm were successfully synthesized using wet chemical process (i.e. chemical precipitation and sol-gel processes). The results showed that variation of citric acid concentration directly influences the particle size and the BET specific surface area. The XRD analysis revealed that nanoparticles were phase pure and that all materials exhibited a tetragonal rutile structure of SnO_2 . Characterisation of the materials was carried out using techniques such as scanning electron microscopy, X-ray diffraction, Fourier Transform Infrared spectroscopy, Thermogravimetric and BET analyses.

1. Introduction

Nano-sized tin oxide (SnO_2) is an interesting semiconducting material with a wide band gap ($E_g = 3.6 \text{ eV}$, at 25°C).^{1,2} Recently, SnO_2 has attracted much attention due to transparency and sensitivity to reducing gases. Nanoparticles of tin oxide have found a wide range of applications in gas sensors, lithium batteries, optoelectronic devices, transparent electrodes and photocatalysts.³⁻⁹ As such the effects of experimental conditions on the chemical and microstructural properties are crucial. For this reason sol-gel and chemical precipitation methods were used in the preparation of SnO_2 nanoparticles. It is general knowledge that by changing the synthesis method it is possible to change the properties of metal oxide particles.¹⁰

One of the most commonly used methods to modify the properties of SnO_2 is variation of surfactant and concentration thereof. This could lead to improved surface area as a result of the formation of small particles of SnO_2 .^{11, 12} It is generally known that increasing the surface/bulk ratio and reducing grain size for rutile SnO_2 nanoparticles has direct benefit in gas sensing.^{13, 14} However, the challenges

associated with sol-gel and chemical precipitation methods are that the products have to be thermally treated at high temperatures to obtain crystalline materials.¹⁵ In the process the surface area decreases whilst the particle size increases due to the particle growth and sintering.¹⁶ In our study citric acid was used in various concentrations to prepare SnO₂ particles with fairly narrow size distribution.

Chemical precipitation and sol-gel methods have been widely used to prepare SnO₂ nanoparticles.^{13, 14, 17, 18} Recently, citric acid assisted sol-gel synthesis and nitrate-citrate gel combustion have been used for the formation of nanoscaled SnO₂ materials.^{13, 18, 19} However, little or no information is available in the literature on the use of citric acid in sol-gel synthesis to control the particle size of SnO₂ nanomaterials.^{20, 21}

Recent studies have shown that nanocrystalline particles with a high surface-to-volume ratio have unique and improved properties.²²⁻²⁴ Furthermore, synthesis of nanomaterials with well controlled size, morphology and chemical composition holds promise in exploring new and enhanced physical properties.²⁵⁻²⁷ In our current study the microstructure of SnO₂ could be controlled by method of preparation and variation of citric acid concentration.

2. Experimental

2.1 Preparation of SnO₂ nanopowders

All reagents were used as received. Tin (IV) chloride pentahydrate (SnCl₄·5H₂O) and citric acid (C₆H₈O₇) were of A.C.S. reagent grade and were both obtained from Aldrich South Africa. Two different methods were used for the synthesis of SnO₂ nanopowders:

2.1.1. Sol-gel procedure²⁸

Appropriate amount of $\text{SnCl}_4 \cdot 5\text{H}_2\text{O}$ was dissolved in distilled water to prepare a clear 0.1 M solution. To this solution 50 ml of different concentrations of citric acid was slowly added with constant stirring and ensuring a total dissolution of citric acid. The concentration of citric acid was varied between 0.01 and 0.5 M. Ammonia solution (32%) was added drop-wise to maintain pH 8-9. The mixture was stirred continuously at room temperature until a sol formed. The sol was evaporated on a water bath that was kept at 80 °C and then dried at 100 °C for 24 hours in an oven to form a xerogel. The xerogel was transferred into a porcelain crucible and pre-annealed at 180 °C for 2 hours to decompose the organic matter completely. Organic-free xerogel was then annealed at 650 °C for 6 hours to form crystalline SnO_2 .

2.1.2. Chemical precipitation²⁸

A 0.1 M solution of tin (IV) chloride was prepared by dissolving appropriate amount of $\text{SnCl}_4 \cdot 5\text{H}_2\text{O}$ in distilled water forming a transparent solution. Ammonia solution ($\text{NH}_3 \cdot \text{H}_2\text{O}$) was added, drop-wise, to the mixture with constant stirring. This was continued until pH 8-9 was attained. The precipitate was formed and washed with distilled water. Then the precipitate was separated from the mixture by centrifugation at the stirring rate of 4500 rpm for 30 minutes at 4 °C. The solid product was dried in air (at room temperature) for overnight and subsequently dried in oven at 100 °C for 24 hours. The product was ground into a fine powder and then annealed at 650 °C for 6 hours.

2.1.3. Sample characterisation

Analysis of the crystallinity of SnO_2 samples was carried out using a PANalytical XPERT-PRO diffractometer. The instrument utilizes Fe filtered $\text{Co K}\alpha$ radiation (1.789 Å). The diffraction patterns were collected with an X-ray gun operated at 35 kV and 50 mA. Raman measurements were carried out using Jobin-Yvon Horiba

T64000 Raman Spectrometer equipped with an Olympus BX-40 microscope. Raman spectrometer configured in triple subtractive mode. The excitation wavelength was the 514.5 nm line from a Coherent Innova 308 argon ion laser. The laser beam diameter at the sample was $\sim 1.5 \mu\text{m}$ whereas the power at the sample was below 1 mW. The specific surface area of the samples was determined by the physical adsorption of a monolayer of nitrogen gas at $-195 \text{ }^\circ\text{C}$ from Brunauer–Emmet–Teller (BET) adsorption measurements using a Micromeritics TRISTAR 3000 analyser. Prior to nitrogen adsorption measurements samples were degassed under vacuum for a few hours. The morphological studies were carried out using Field Emission-Scanning Electron Microscopy (FE-SEM) on a JEOL 7500F SEM. Thermal analysis studies were carried out using a Perkin Elmer thermogravimetric analyser (TGA). Samples were purged with either nitrogen or oxygen and heated from room temperature to $800 \text{ }^\circ\text{C}$ at a heating rate of $10 \text{ }^\circ\text{C}/\text{min}$.

3. Results and discussion

The Physico-chemical properties of SnO_2 samples prepared by both Sol-gel and chemical precipitation procedures are reported in **Table 1**. The specific BET surface area of sample prepared by chemical precipitation process (CP) was found to be the largest ($29 \text{ m}^2/\text{g}$). The addition of citric acid (SG1, SG2, SG3, SG4 and SG5) resulted in a decrease in specific BET surface area (from 29 to $0.2 \text{ m}^2/\text{g}$) and an increase in average pore diameter. The decrease in surface area is more noticeable as the concentration of citric acid is increased (0.01 to 0.5M). This is mainly thought to be due to possible penetration of the dispersed citrate into the pores of SnO_2 . This could also mean that citric acid promotes agglomeration of SnO_2 particles leading to a decrease in BET specific surface area. At the calcination temperature ($650 \text{ }^\circ\text{C}$ for 6 hours) the amount of citrate retained on the surface of SnO_2 is decreased for all citric

acid-treated samples. The decrease is attributed to the decomposition of citrate moieties from the surface of SnO₂. This suggests that the surface groups could come together and condense to form a densely packed SnO₂ lattice. This could lead to a decrease in surface area and the effect is more pronounced for higher concentrations of citric acid.

The pore volume of citric acid-treated samples decreased with a decrease in specific BET surface area which clearly suggests that the decrease in BET surface area is directly influenced by the pore volume (porosity).

Nitrogen adsorption-desorption isotherms of citric acid-treated SG1 is shown in **Fig. 1**. Isotherms of other citric acid-treated samples (i.e. SG2, SG3, SG4 and SG5) were also found to be similar (not shown). The isotherms could be classified as type IV with straight H3 hysteresis loop above $P/P_0 \approx 0.6$ which is characteristic of slit-shaped pores.¹⁰ This suggests that that the textural properties are influenced by external surface area. The flat and slightly concave curve in the low relative-pressure domain, $P/P_0 < 0.2$, is due the presence of very small microporosity. This type of adsorption-desorption isotherm is typical of clay minerals wherein nitrogen physisorption occurs between the aggregates of platelet particles.¹⁰

The pore size distribution plot calculated using the Barrett–Joyner–Halenda (BJH) equation from the adsorption branch of the isotherm is shown in **Fig. 1** (inset). The material showed a relatively narrow pore size distribution (centred at 38 nm) suggesting good homogeneity of the pores.

CP showed a hysteresis loop different from the citric acid-treated samples (SG1-SG5). For this sample (CP) the hysteresis loop is changed from H3 to H1 type and this is supported by the pore size distribution which is found to be narrower (centred at 8 nm) than those of samples SG1-SG5.

Table 1: Physico-chemical properties of SnO₂ materials prepared by sol-gel and chemical precipitation processes.

Sample	Designation	S _{BET} (m ² /g)	Pore size (Å)	Pore volume (cm ³ /g)
CP	CP	29.25	10.29	0.077
SG-0.01M	SG1	21.50	14.22	0.188
SG-0.05M	SG2	15.11	15.70	0.098
SG-0.1M	SG3	8.69	18.86	0.041
SG-0.2M	SG4	4.27	24.77	0.027
SG-0.5M	SG5	0.24	25.77	0.002

SG = Sol-gel; CP = Chemical precipitation; S_{BET} = BET Surface area

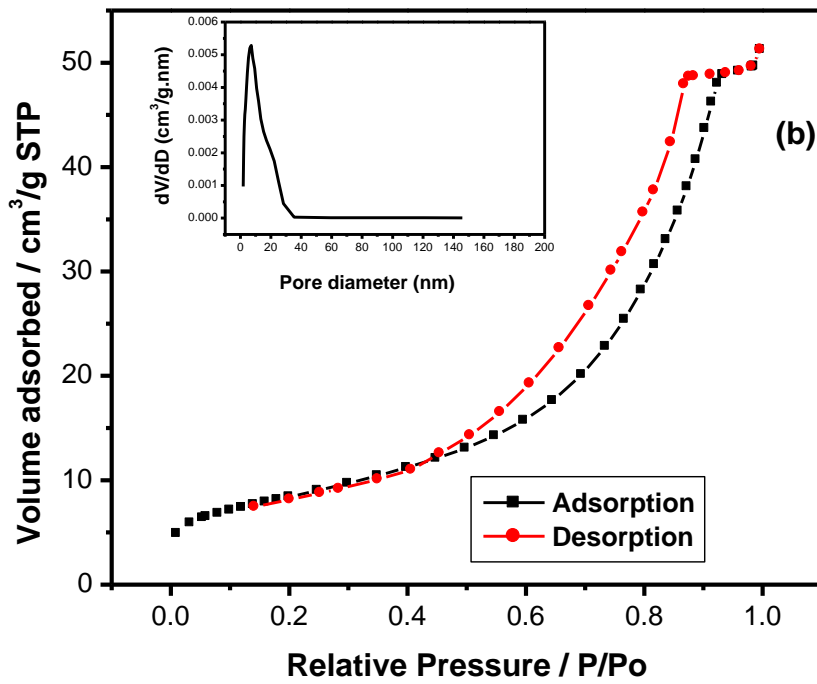
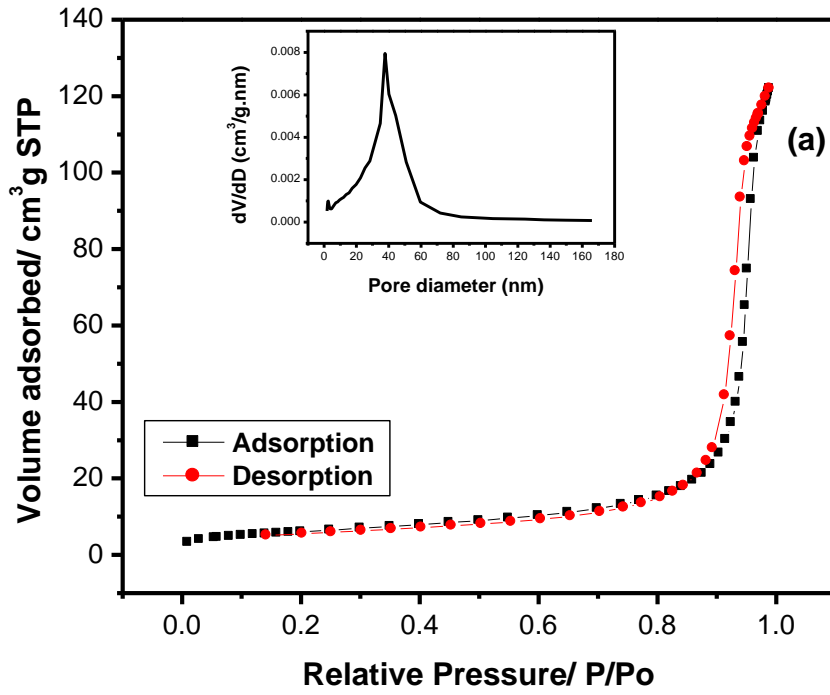


Fig. 1. Nitrogen adsorption–desorption isotherms and corresponding pore size distributions (insets) of CP (a) and SG1 (b).

The surface morphology of the sample prepared by chemical precipitation procedure (prepared in the absence of citric acid) was studied under the electron microscope and the typical SEM image is shown in **Fig. 2**. The SEM image shows that CP is mainly composed of clusters of small agglomerated particles with somewhat uniform and spherical morphology. SEM images in **Fig. 3** show the effect of concentration of citric acid on the microstructure evolution of Sol-gel synthesized materials (SG1-SG5). It was found that lower citric acid concentration (SG1) gave spherical shape morphology with uniform particle size. However, increasing the concentration of citric acid resulted in particle growth and the formation of somewhat spherical but irregular morphology (SG5). The SEM images suggest that the acid treatment step (citric acid) promotes particle aggregation and subsequently the deformation of particle morphology (**Fig. 3e**). The decrease in the number of spherical particles at higher citric acid concentration is attributed to particle aggregation induced by the citrate. This is particularly in agreement with the BET results that showed a sharp decrease in surface area with the increase in citric acid concentration. It is noteworthy that all citric acid-treated samples revealed a relatively smaller surface area and larger particle size compared to CP. This suggests that the presence of citrate moiety promotes aggregation possibly by inducing charge accumulation on the surface leading to particles sticking together to form bigger particles. Zhijie Li et al. reported on the effects of citric acid on hydrothermally-prepared SnO₂. In their study the presence of citric acid led to the formation of materials with larger surface area.¹⁰ However, in our study the presence of citric acid in different concentration led to a

sharp decrease in surface area. This clearly shows that the effects of citric acid are dependent on the method of preparation.

Not only does the variation of concentrations of citric acid lead to grain growth but morphological transformation too. SnO₂ particles transformed from regular sphere to irregular sphere and subsequently to polyhedron shape with an increase in citric acid concentration (i.e. 0.01 to 0.5M). The formation of polyhedron shape is thought to be due to self assembly of smaller particles. Self assembly growth is mediated by thermodynamics of the system and it is also time dependent. The presence of a chelating agent in the solution slows down the reaction and allows more time for growth after the nucleation process. The bigger grains have an overall reduced surface energy which is thermodynamically favourable. This clearly shows that citric acid influences the nucleation process and subsequently grain growth.

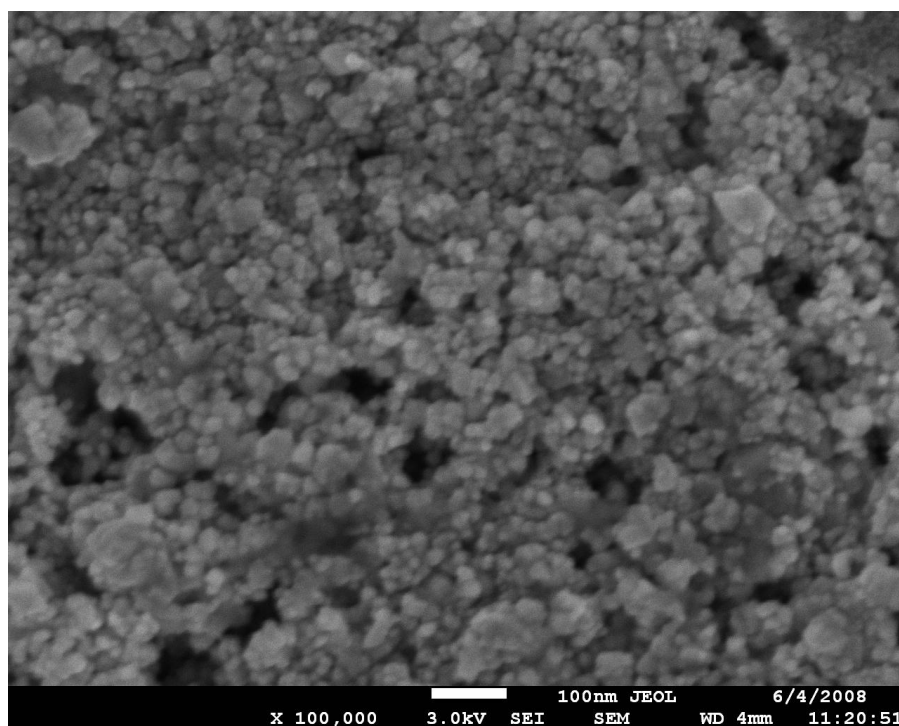


Fig. 2. SEM micrograph of CP

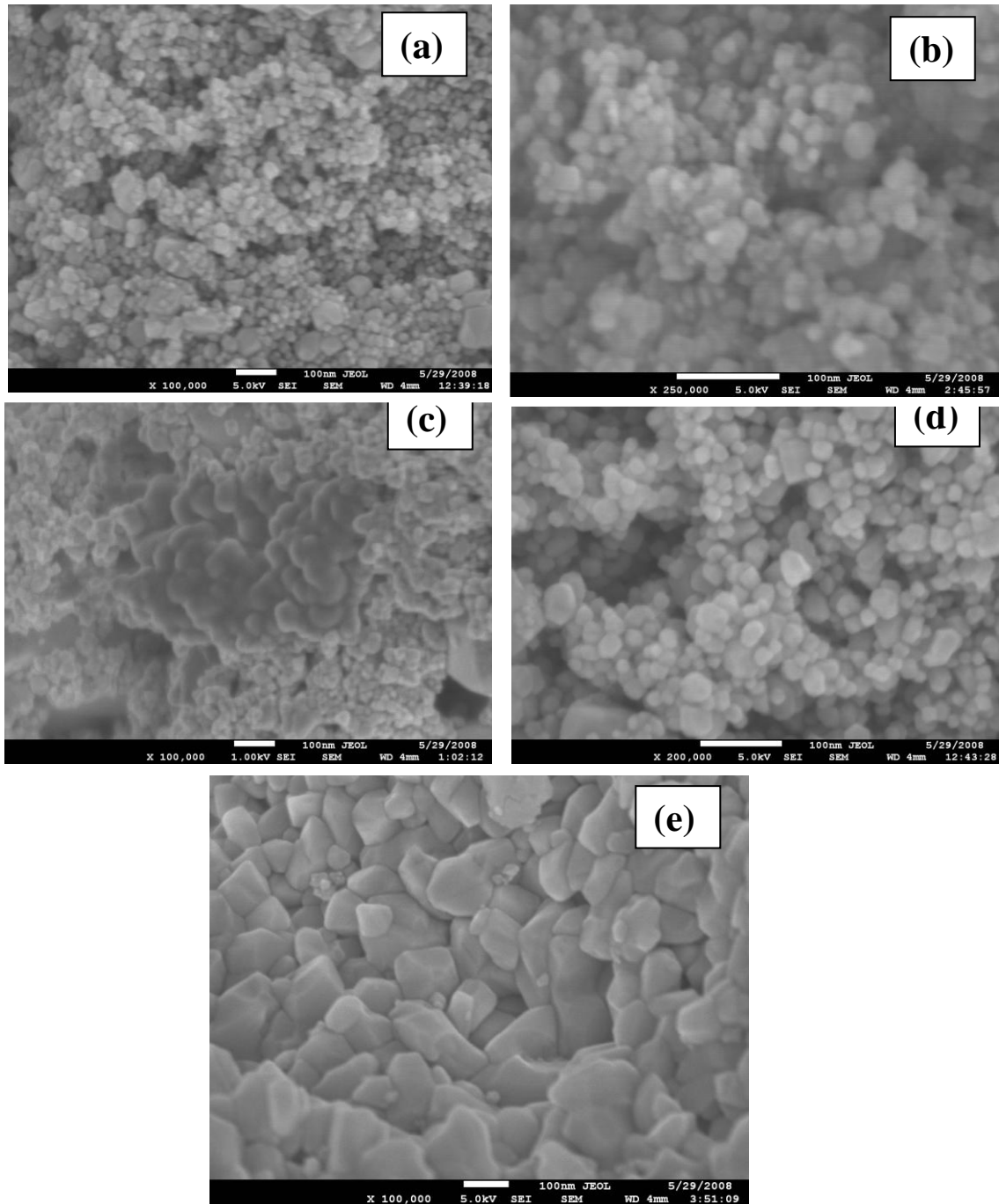


Fig. 3. SEM micrographs of (a) SG1, (b) SG2, (c) SG3, (d) SG4 and (e) SG5

The energy dispersive X-ray (EDX) spectrum of sample SG1 is shown in **Fig. 4**. All samples gave similar EDX spectra (not shown). EDX spectrum revealed that the material is only composed of Sn and O atoms. This shows that the citrate moiety was completely removed during the washing step.

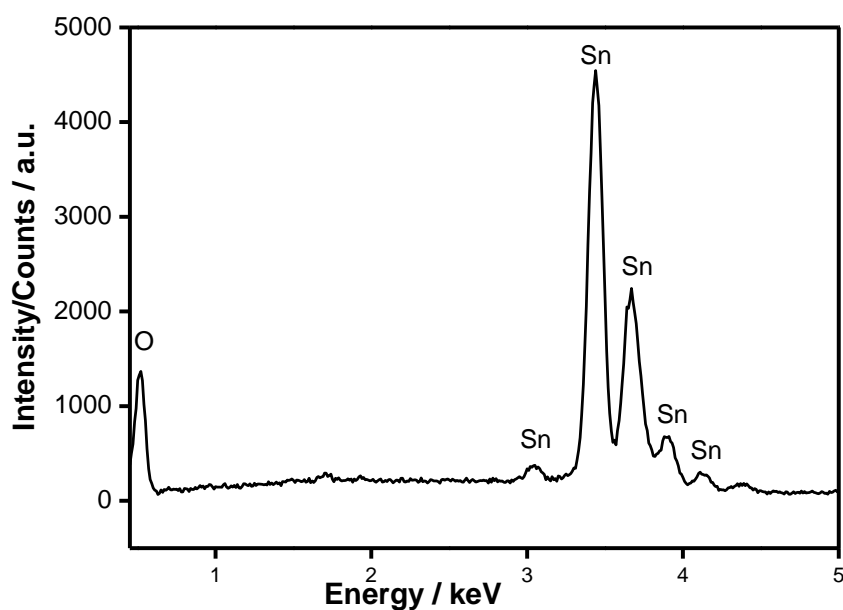


Figure 4: EDX spectrum of SG1.

The relationship between the concentration of citric acid and particle size as determined by SEM is shown in **Fig. 5**. It can be seen that average particle size of SnO₂ increases with an increase in citric acid concentration. The average particle size ranges from 19 nm (for 0 M citric acid, CP) to about 100 nm (for 0.5 M citric acid, SG5). It is noteworthy that in the case of citric acid treated samples when citric acid concentration was increased 50 times (0.01 to 0.5 M) the particle size became 5 times larger (22 to 100 nm). This clearly shows citric acid plays a role in the growing mechanism of SnO₂ particles.

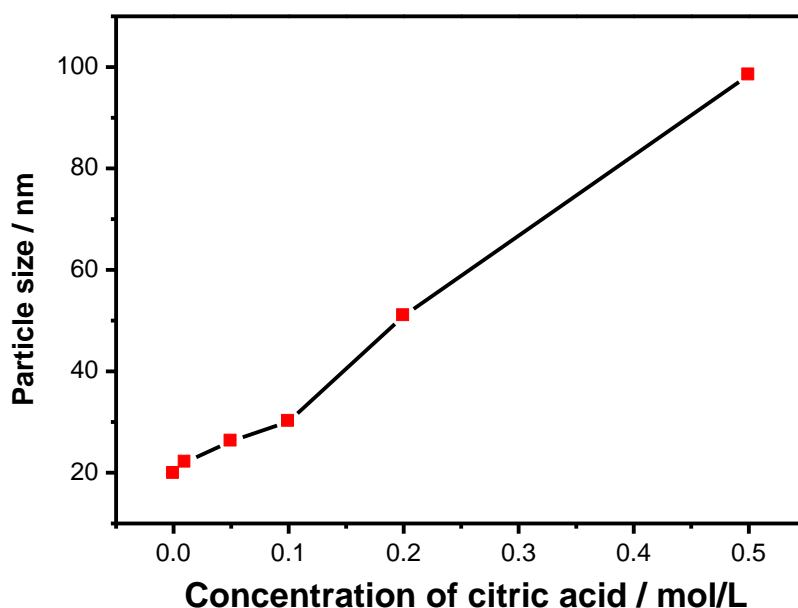


Fig. 5. Effects of concentration of citric acid on the particle size

XRD

The XRD patterns of chemical precipitation synthesized (CP) and sol-gel prepared samples (SG1-SG5) are shown in **Fig. 6**. CP showed similar diffraction peak position to that of citric acid treated samples (SG1-SG5). These peaks could all be indexed to a tetragonal rutile phase of SnO₂ (JCPDS card No. 41-1445).²⁹ This shows that all materials prepared are phase pure and that treatment with citric acid does not influence the crystal structure of SnO₂. However, CP showed broader peaks than citric acid treated samples. Peak broadening became more pronounced as the concentration of citric acid decreased. Thus, crystallinity of SnO₂ increases with increasing concentration of citric acid as shown by increasing peak intensity. This phenomenon is attributed to grain growth. This is in agreement with BET results and particle size calculated from SEM. The absence of citric acid resulted in smaller grain size whereas larger concentration of citric acid resulted in larger particles and smaller surface area.

The average crystal size of the nanoparticles was confirmed using the Scherrer equation:

$$d = \frac{K\lambda}{\beta \cos\theta}$$

where d is the mean crystalline size, K is a grain shape dependent constant (0.9), λ is the wavelength of the incident beam, θ is the Bragg reflection angle and β is the full width half maximum. The crystalline size estimated from the XRD spectra using the Scherrer was in the range of 16 nm to 33 nm as the concentration of citric acid was increased. The data from both techniques suggest an increase in both crystalline and particle size as the concentration of citric acid was increased.

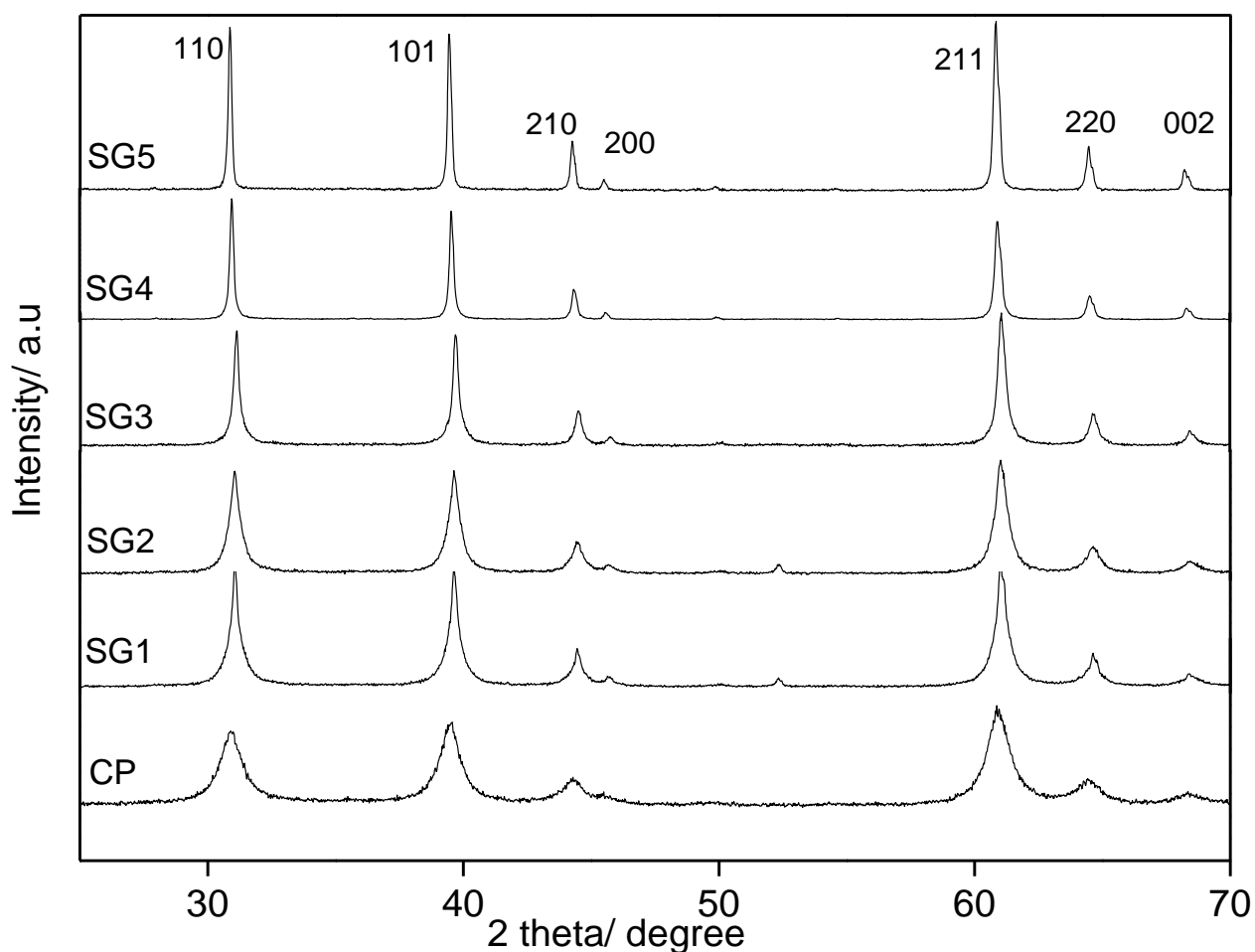


Fig. 6. XRD patterns of CP, SG1, SG2, SG3, SG4 and SG5.

Raman

Structural comparison between CP and SG series samples is revealed by the Raman results (**Fig. 7**). The CP profile revealed the presence of two main bands at 633 and 774 cm^{-1} which are assigned to a tetragonal rutile structure of SnO_2 material.³⁰ The broader and relatively weaker bands are due to the poor crystallinity of the CP sample. These peaks might have shifted due to the size effect. More peaks were observed for citric acid treated samples. This was more pronounced for higher concentrations of citric acid. The characteristic rutile bands are observed for the acid treated samples at 244, 475, 633 and 774 cm^{-1} . The more intense bands observed for SG5 are indicative of the crystalline nature of the sample and this is due to larger crystal size. This shows that citric acid did not have influence on the crystal structure but crystal size. The increase in intensity with increasing concentration suggests that citric acid does not interact strongly with SnO_2 and that this interaction enhances crystallization. Both the XRD and Raman results show that all materials are phase pure.

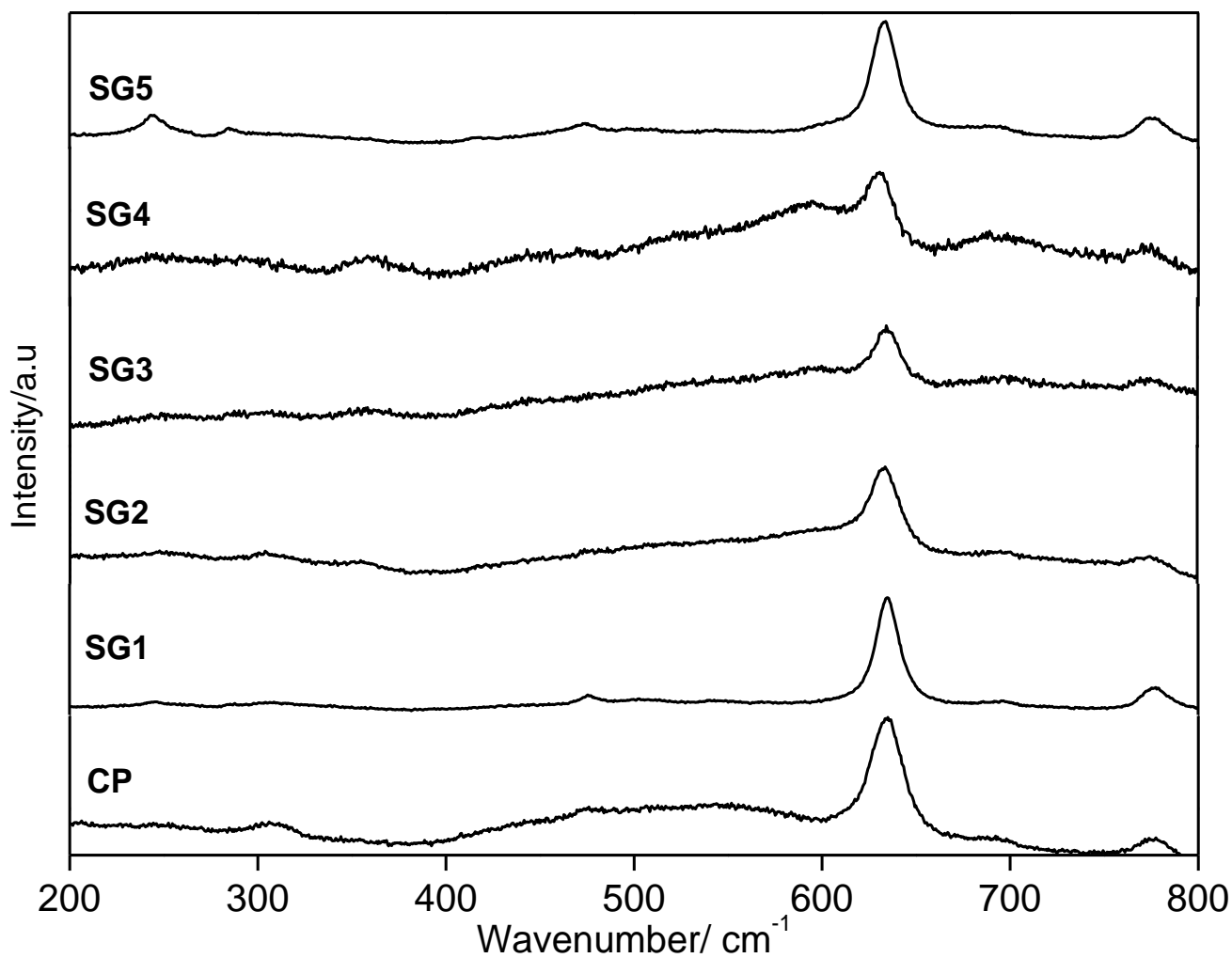


Fig. 7. Raman spectra of CP and citric acid treated samples (SG1-SG5)

FTIR

FTIR spectra of CP and SG series (SG1-SG5) samples are shown in **Fig. 8**. All samples showed similar spectra. The small absorption peak observed at 3400 cm^{-1} is attributed to hydroxyl groups.³¹ This is mainly due to the adsorbed water retained by SnO_2 . The spectra were not recorded in situ and so the absorption of water or CO_2 from the ambience might have occurred.^{32, 33} Furthermore, peaks observed at 1095 and 605 cm^{-1} are assigned to the fundamental vibrations of Sn-O. These bands correspond to the antisymmetric Sn-O-Sn stretching mode. The molecular vibrations

of chemical bonds observed are all associated with SnO₂ and this shows the purity of the materials.

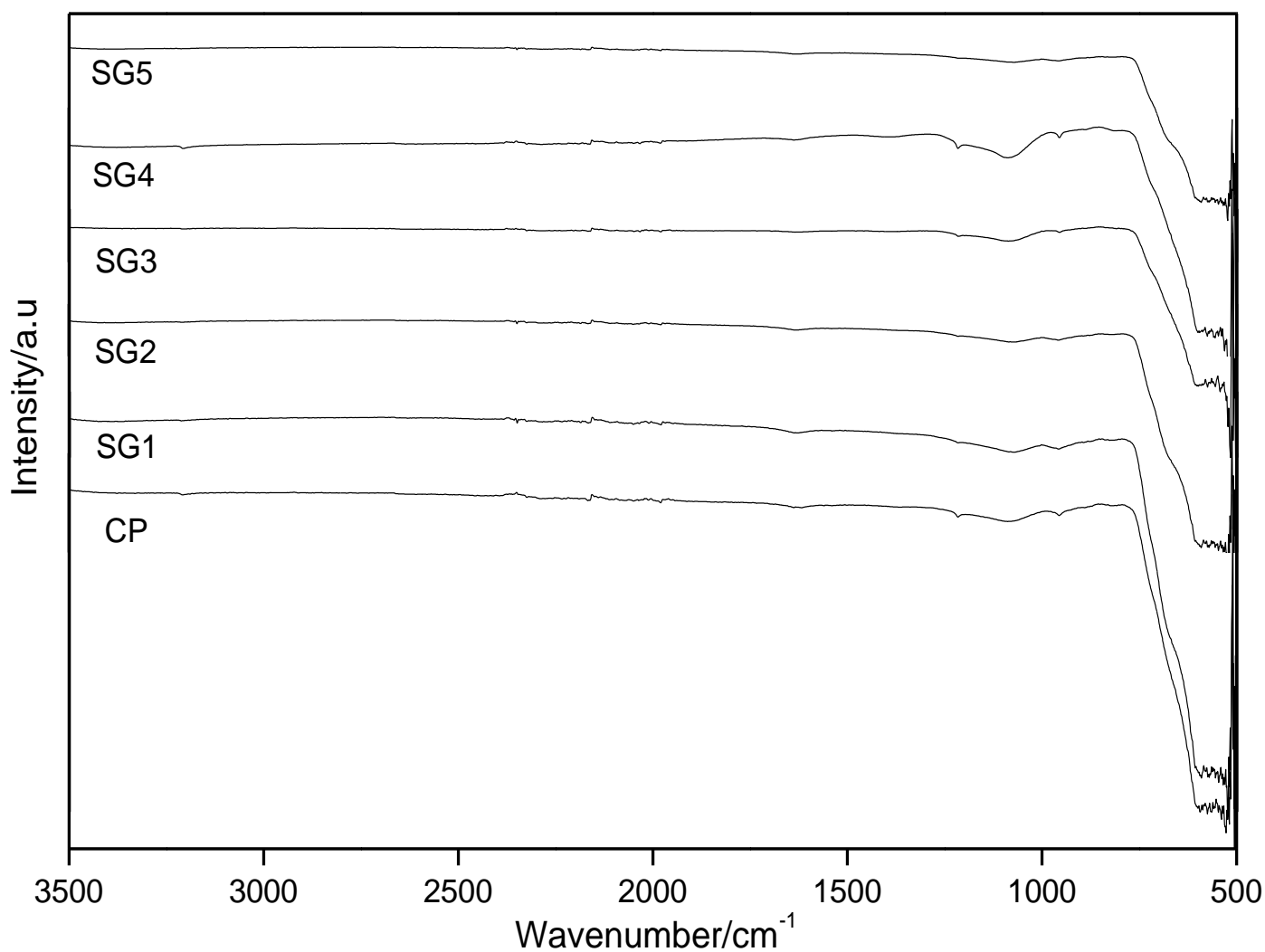


Fig. 8. FTIR spectra of CP and SG series samples

TGA

In order to monitor the structural changes in the samples as a result of temperature elevation, thermogravimetric analysis (TGA) was carried out in the temperature range of 20 to 800 °C (**Fig. 9**). The TGA profiles of the samples were collected under oxygen and nitrogen ambiences. However, the profiles of CP and those of SG series

samples were found to be similar under both ambiances. As such only CP and SG1 profiles collected under nitrogen atmosphere are shown in **Fig. 9**.

The first observed weight losses beginning at ~ 20 °C and ending at ~ 100 °C (~ 0.5 %) for both CP and SG1 are attributed to the loss of physically adsorbed water. The second weight losses observed between ~ 250 and ~ 650 °C are due to the dehydroxylation of the particle surface and boundaries occurring at the same time.³⁴

The total weight loss of about 1 % for both CP and SG series samples was observed and is indicative of the absence of residual organic compounds. This shows that sample washing and calcination (650 °C) steps effectively removed the citrate and chloride moieties. This finding is in accordance with the EDX and FTIR results.

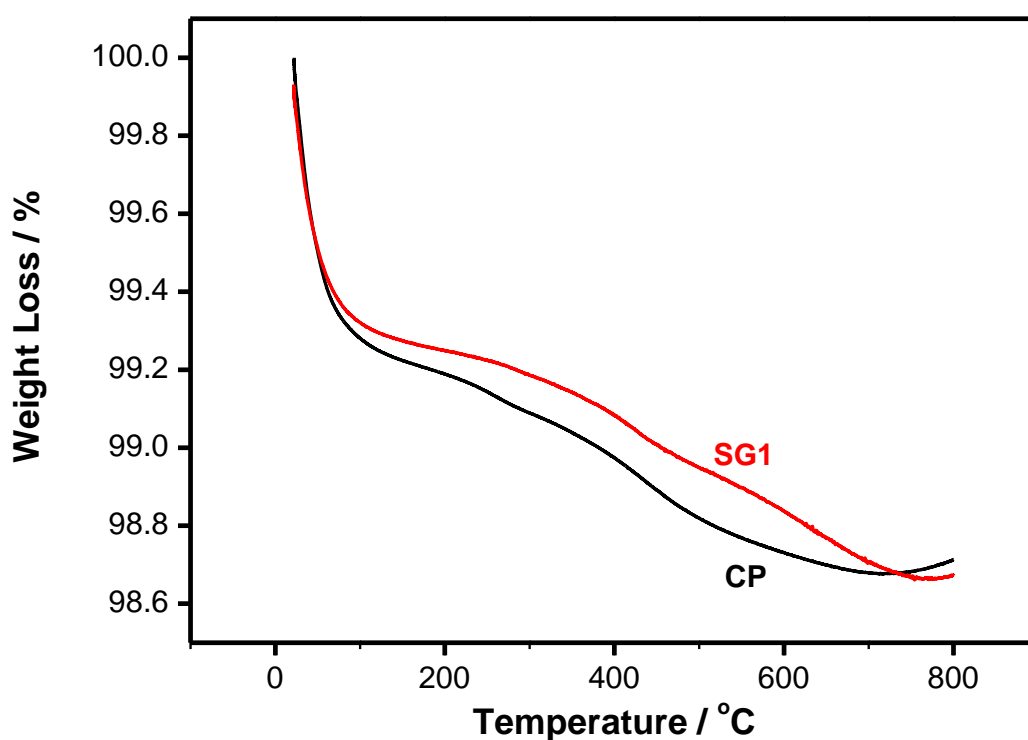


Fig. 9. TGA profiles of CP and SG1 samples collected under nitrogen ambience

4. Conclusions

SnO₂ samples were prepared using chemical precipitation and sol-gel methods. With both methods it was possible to obtain SnO₂ nanoparticles with narrow size distribution. However, chemical precipitation produced particles relatively smaller than those of sol-gel process. Furthermore, the surface area was found to be larger for particles synthesized by chemical precipitation. There is evidence of particle aggregation during heat treatment. Treatment with citric acid resulted in grain growth and reduced surface area which implies reduced surface energy. This phenomenon is thermodynamically favoured. Both methods produced materials free from chemical contamination. All samples were found to correspond to tetragonal rutile phase of SnO₂. This clearly shows that annealing samples at 650 °C could effectively remove the chloride and nitrate ions.

Acknowledgement

The authors thank the Council for Scientific and Industrial Research and the Department of Science and Technology, South Africa, for the financial support.

References

1. F. Gu, S.F. Wang, M.K. Lu, Y.X. Qi, G.J. Zhou, D. Xu, D.R. Yuan, *Opt. Mater.* 25, 59 (2004)
2. T. Hayakawa and M. Nogami, *Sci. Technol. Adv. Mater.* 6, 66 (2005)
3. S. Chappel and A. Zaban, *Sol. Energ. Mat. Sol. Cells.* 71, 141 (2002)
4. M.C. Schlamp, X. Peng and A.P. Alivisatos, *J. Appl. Phys.* 82, 5837 (1997)
5. A. Cirera, A. Vila, A. Dieguez, A. Cabot, A. Cornet and J.R. Morante, *Sens. Actuat. B* 64, 65 (2000)
6. M. Miyauchi, A. Nakajima, T. Watanabe and K. Hashimoto, *Chem. Mater.* 14, 2812 (2002)

7. J. Morales, V.C. Perez, S. Santos and L.J. Tirado, *J. Electrochem. Soc.* 143, 2847 (1996)
8. D. Aurbach, A. Nimberger, B. Markovsky, E. Levi, E. Sominski and A. Gedanken, *Chem. Mater.* 14, 4155 (2002)
9. M.V. Artemyev, V. Sperling and U. Woggon, *J. Appl. Phys.* 81, 6975 (1997)
10. Z. Li, W. Shen, X. Zhang, L. Fang and X. Zu, *Colloids Surf. A: Physicochem. Eng. Aspects* 327, 17 (2008)
11. Y. Wang, C. Ma, X. Sun and H. Li, *Inorg. Chem. Commun.* 5, 751 (2002)
12. L. Zhu, Z. Jia and Y. Tang, *Chin. J. Chem. Phys.* 18, 237 (2005)
13. F. Gu, S.F. Wang, M.K. Lu, Y.X. Qi, G.J. Zhou, D. Xu and D.R. Yuan, *Inorg. Chem. Commun.* 6, 882 (2003)
14. D. Kotsikau, M. Ivanovskaya, D. Orlik and M. Falasconi, *Sens. Actuat. B* 101, 199 (2004)
15. Y. Liang, J. Fan, X. Xia and Z. Jia, *Mater. Lett.* 61, 4370 (2007)
16. S. Fujihara, T. Maeda, H. Ohgi, E. Hosono, H. Imai and S.-H. Kim, *Langmuir* 20, 6476 (2004)
17. M. Kakihana, *J. Sol-Gel Sci. Technol.* 6, 7 (1996)
18. N.-S. Baik, G. Sakai, N. Miura and N. Yamazoe, *J. Am. Ceram. Soc.* 83, 2983 (2000)
19. Q.H. Cao, Y.Q. Gao, X.Y. Chen, L. Mu, W.C. Yu and Y.T. Qian, *Chem. Lett.* 35, 178 (2006)
20. L. Fragi, D.G. Lamas and N.E. Walsoe de Reca, *Nanostruct. Mater.* 11, 311 (1999)
21. M. Bhagwat, P. Shah and V. Ramaswamy, *Mater. Lett.* 57, 1604 (2003)
22. N. Yamazoe, *Sens. Actuat. B* 5, 7 (1991)

23. A. Gurlo, M. Ivanovshaya, N. Barsan, M. Schweizer-Berberich, U. Weimar, W. Gopal and A. Dieguez, *Sens. Actuat. B* 44, 327 (1997)
24. N. Pinna, G. Neri, M. Antonietti and M. Niederberger, *Angewandte Chemie International Edition* 43, 4345 (2004)
25. C.G. Granqvist and A. Hultaker, *Thin Solid Films* 411, 1 (2002)
26. Y. Wang and N. Herron, *J. Phys. Chem.* 95, 525 (1991)
27. A.P. Alivisatos, *J. Phys. Chem.* 100, 13226 (1996)
28. X Lou, C. Peng, X. Wang and W. Chu, *Vacuum* 81, 883 (2007)
29. K.S.W. Sing, D.H. Everett, R.A.W. Haul, L. Moscou, R.A. Pierotti, J. Rouquerol and T. Sieminiowska, *Pure Appl. Chem.* 57, 603 (1985)
30. P. S. Peercy and B. Morosin, *Phys. Rev. B* 7, 2779 (1973)
31. R.M. Silverstein and F.X. Webster, *Spectrometric Identification of Organic Compounds*, sixth ed. John Wiley & Sons Inc Publications, New York (2007)
32. S. Emiroglu, N. Barsan, U. Weimar and V. Hoffmann, *Thin Solid Films* 391, 176. (2001)
33. B. Orel, U. Lavrencic-Stankgar, Z. Crnjak-Orel, P. Bukovec and M. Kosec, *J. Non- Cryst. Solids* 167, 272 (1994)
34. K.C. Song and Y. Kang, *Mater. Lett.* 42, 283 (2000)